Preparation and Structure of Ruthenium Tetrafluoride and a Structural Comparison with Ruthenium Trifluoride and Ruthenium Pentafluoride‖

William J. Casteel, Jr.,† Angus P. Wilkinson,‡ Horst Borrmann,† Robert E. Serfass,§ and Neil Bartlett*,†

Chemical Sciences Division, Lawrence Berkeley Laboratory, and Department of Chemistry, University of California, Berkeley, California 94720, Department of Chemical Crystallography, The University of Oxford, Oxford, England OX1 3PD, and Chemistry Department, Princeton University, Princeton, New Jersey 08540

Received September 24, 1991

A new synthetic approach has provided RuF_4 as a deep pink polycrystalline solid from the interaction of AsF_5 with RuF_6^{2-} in anhydrous hydrogen fluoride solution. The structure has been determined from a combination of X-ray synchrotron and neutron powder diffraction data. The unit cell, refined from the neutron data, is monoclinic with $a = 5.6068$ (6) Å, $b = 4.9456$ (5) Å, $c = 5.413$ (2) Å, $\beta = 121.27$ (2)°, $V = 128.3$ Å^3, $Z = 2$, and space group $P2_1/n$. Each Ru atom has six near-neighbor F ligands on an octahedral framework, four in the same plane, each shared with another Ru atom, to form a puckered-sheet array. The fluorine-bridge bonding is very similar to that which occurs in RuF_3 and in the tetrameric molecule $(RuF_5)_4$. The structure of RuF_3 has been confirmed from X-ray powder data on samples prepared by pyrohydrolysis of SF_3RuF_6. The structure of RuF_5 has been redetermined for this comparison and found to have a monoclinic unit cell with $a = 5.4969$ (6) Å, $b = 9.946$ (1) Å, $c = 12.531$ (2) Å, $\beta = 99.98$ (1)°, $V = 674.7$ (2) Å^3, and $Z = 8$. The bridging interatomic distances in the three fluorides are as follows: RuF_3, 1.982 (6) Å; RuF_4, 2.00 (1) and 2.00 (3) Å; RuF_5, 1.995 (1), 1.999 (1), 2.003 (1), and 2.007 (1) Å. The Ru–F–Ru angles are as follows: RuF_3, 136 (1)°; RuF_4, 133 (1)°; RuF_5, 136.8 (1) and 140.8 (1)°. The nonbridging F ligands in RuF_4 are trans to one another, above and below the Ru in the sheet array. The puckered sheets are packed with the nonbridging F ligands nestling in holes, in the array of such ligands of the adjacent sheet. The RuF_4 restrained nonbridging interatomic distance, Ru–F = 1.82 (2) Å, matches those in $(RuF_5)_4$ perpendicular to the eight-membered ring, where the interatomic distances are 1.817, 1.821, 1.823, and 1.824 Å (all occurring twice, with $\sigma = 0.001$ Å). The equatorial nonbridging Ru–F distances are significantly shorter, with two each at 1.793, 1.795, 1.796, and 1.798 Å (all $\sigma = 0.001$ Å).

Introduction

Structural information on transition-metal binary fluorides[1-3] shows that from group V through to the end of each transition series the transition-metal atom is coordinated by six fluorine ligands (F) on an octahedral framework. This is so for hexafluorides, pentafluorides, tetrafluorides, or trifluorides.

The necessary bridging fluorine ligands (F_b), of which there are two in the pentafluoride, four in the tetrafluoride, and six in the trifluoride, are usually symmetrically linked to the two metal atoms that they join. Although much of the available data is not precise, it appears that the bridging-fluorine to metal distances ($M–F_b$) are, generally, approximately 0.2 Å longer than the nonbridging ($M–F_{nb}$).

Whenever antibonding σ (σ^*) orbitals are occupied, the anticipated weakening of the σ bonds is manifest[4] in longer M–F interatomic distances and greater formula unit volumes than those of earlier members of the transition series, in which the σ^* orbitals are vacant. In addition, when the σ^* orbitals are not of equal occupancy, gross distortion (Jahn–Teller) occurs.[4] In the second and third transition series, where higher ligand fields prevail, the σ^* orbitals remain vacant through to RhF_3 and IrF_3. For these and earlier binary fluorides of each transition series, in all known oxidation states, the pseudooctahedral arrangement of the six F ligands about each M is tightly bound. All of this is in conformity with simple ligand field theory. Unexpectedly, however, the available (and often imprecise) data indicate that the interatomic distances of the same type (either $M–F_b$ or $M–F_{nb}$) do not depend upon the oxidation state of M.

The antibonding $\pi(\pi^*)$ effect of the dt_{2g} configuration of a metal pentafluoride must be less than in the case of the trifluoride of that element, where the π^* population is greater by two electrons. A recent single crystal structure determination of RhF_3 by Grosse and Hoppe,[5] however, has shown that the interatomic distance, $Rh–F_b = 1.961$ (2) Å, is significantly shorter than the bridging distances in $(RhF_5)_4$, found by Morrell et al.,[6] which range from 1.993 (4) to 2.005 (3) Å. Similarly, the structure of the pressure-stabilized perovskite trifluoride of niobium, as described by Pouchard et al.,[7] has $Nb–F_b = 1.970$ (1) Å, which is shorter than that given by Edwards,[8] for the bridging distances in $(NbF_5)_4$, where $Nb–F_b = 2.06$ (2) and 2.07 (2) Å.

Unfortunately, much of the other available data[1-3] on the transition-element binary fluorides is so imprecise that the generality of the unexpected slight *decrease* in $M–F_b$ with *decrease* in oxidation state is not convincingly demonstrated. Knowledge of the impact of oxidation state on the nonbridging interatomic distances is even less well defined. To respond to these questions, and to the related one of the impact of oxidation state on the bridging angle $M–F_b–M$, a reliable set of accurate structures for the penta-, tetra-, and trifluorides of one of these metals was needed.

† University of California.
‡ University of Oxford.
§ Princeton University.
‖ Dedicated to Professor Rudolf Hoppe on the occasion of his 70th birthday.

(1) Edwards, A. J. *Adv. Inorg. Radiochem.* **1983**, *27*, 83.
(2) Babel, D.; Tressaud, A. In *Inorganic Solid Fluorides*; Hagenmüller, P., Ed.; Academic Press, Inc.: New York, 1985; pp 78–204.
(3) Müller, B. G. *Angew. Chem., Int. Ed. Engl.* **1987**, *26*, 1081.
(4) Einstein, F. W. B.; Rao, R. R.; Trotter, J.; Bartlett, N. *J. Chem. Soc. A* **1967**, 478.
(5) Grosse, L.; Hoppe, R. *Z. Anorg. Allg. Chem.* **1987**, *552*, 123.
(6) Morrell, B. K.; Zalkin, A.; Tressaud, A.; Bartlett, N. *Inorg. Chem.* **1973**, *12*, 2640.
(7) Pouchard, M.; Torki, M. R.; Demazeau, G.; Hagenmüller, P. *C. R. Hebd. Sceances Acad. Sci.* **1971**, *C273*, 1093.
(8) Edwards, A. J. *J. Chem. Soc.* **1964**, 3714.

0020-1669/92/1331-3124$03.00/0

The binary fluorides of ruthenium were selected for several reasons. Greater structural precision from X-ray diffraction data was more likely than from a third transition series set of fluorides. Four binary fluorides (a hexa-,[9] penta-,[10] tetra-,[11] and trifluoride[12]) of ruthenium were known to be preparable, and the structure of the tetrafluoride was of special interest.

It was known from X-ray powder diffraction patterns, obtained[13] by an adaption of the original preparation[11] of RuF_4, that it was not isostructural with either NbF_4 (the structure of which had been shown[14,15] to be of SnF_4 type[16]) or[17] with OsF_4. The X-ray powder pattern of OsF_4 proved to be very like that of RhF_4 and to be structurally related to PdF_4,[18] which is the structure also adopted[19] by PtF_4 and IrF_4. OsF_4 had been prepared in these laboratories by a novel synthetic route,[17] which was also effective in making RuF_4. This synthetic route provided RuF_4, free of the other polymeric fluoride, RuF_3. This promised to give powder diffraction data for a structure determination of adequate precision for the purposes of this study.

At the outset of this study it was recognized that oxygen contamination had probably contributed to the structural imprecision in some of the earlier work. Such contamination, in the form of $RuOF_4$ dissolved in the RuF_5, could have contributed to the low precision in the previous structure determinations[10,20] of RuF_5 since Holloway and Peacock have demonstrated[21] that the early procedure[22] for preparing RuF_5, via the interaction of BrF_3 with ruthenium in glass containers, also produces $RuOF_4$. Indeed this may also, at least in part, account for the variation in unit cell parameters and composition noted by Jack and his co-workers[12] for the various samples of RuF_3, each prepared by reducing "RuF_5" with a different agent.

In the present study, all syntheses have been designed to avoid oxygen ligand access to the ruthenium atom. This has entailed the design of a new route to salts of RuF_6^{2-}, as a precursor to RuF_4. RuF_3 has been prepared by the internal redox involved in the pyrolysis of the salt $SF_3^+RuF_6^-$.

The structure of the tetrafluoride has proved to be similar to that of VF_4 as recently described[23] by Becker and Müller, the structural unit being closely related to that of the $(RuF_5)_4$ tetrameric unit, which is now more precisely defined. In addition the structural parameters selected by Jack and his co-workers,[12] as appropriate for stoichiometric RuF_3, have been confirmed and the structure shown to have a close affinity with bridging features of the penta- and tetrafluorides.

Experimental Section

Reagents. Powdered *ruthenium*, supplied by Alfa Products, Thiokol, Danvers, MA 01923, was reduced in hydrogen at 450 °C for 6 h and not again exposed to the air prior to fluorination. *Fluorine* and *BF_3* were used as supplied by Matheson Gas Products, East Rutherford, NJ 07073. Anhydrous hydrogen fluoride (Matheson) was held at ~20 °C, as the liquid, in a Teflon tube with Teflon valve, over solid K_2NiF_6 (Ozark Mahoning, Tulsa, OK) to remove water. SF_4, PF_5, AsF_5, and BrF_3 were each used as supplied by Ozark Mahoning.

Apparatus and Technique. RuF_5, SF_3RuF_6, and RuF_3 were prepared in all-welded Monel cans by procedures akin to those previously described,[24] but for the synthesis of RuF_4, Teflon tubes and valves were employed, as in the synthesis[25] of AgF_3. Fluorine and gaseous fluorides were handled in a stainless steel or Monel vacuum line.[25] Translucent fluorocarbon polymer tubing (FEP) was obtained from CHEMPLAST Inc., Wayne, NJ 07470. Whitey valves (1KS4) were obtained from Oakland Valve and Fitting Co., Walnut Creek, CA 94596. All solid fluorides were manipulated in the dry Ar atmosphere of a Vacuum Atmospheres Corp. Dri-lab.

Powder diffraction samples were prepared as previously described.[25] The powder was vibrated down the capillary by drawing a lightweight file across it and was finally tamped into a well-packed column with a quartz ramrod drawn to fit the 0.5- or 0.3-mm capillaries used for the samples. For the neutron diffraction experiments, 2-mm o.d. capillaries joined to a $^1/_4$-in. o.d. tube and connected to a Whitey valve were similarly filled to a length of 35 mm. Loaded capillaries were plugged with dry KelF grease, removed from the Dri-lab, and sealed by drawing down in a small flame.

RuF_5 Preparation and Structure. In the Dri-lab 300 mg of Ru powder was loaded into a small nickel vessel and placed into a 250-mL Monel can which had been passivated with 4 atm of F_2 at 250 °C for 24 h. The can was fitted with a valved lid, which could be cooled during the experiment, and evacuated to better than 10^{-2} Torr on a stainless steel vacuum line. F_2 (4 atm) was admitted, and the can was slowly heated to 250 °C and held at this temperature for 24 h, the lid being cooled with cold water. On cooling of the can to room temperature, the remaining F_2 was evacuated through a glass U-trap, cooled to −196 °C, into a soda-lime scrubber. A small amount of RuF_6 (red-brown) was collected in the U-trap. The can was opened in the Dri-lab, revealing waxy, lime-green RuF_5 on the lid and cooler portions of the can. For crystal growth, the RuF_5 was loaded into a flame-dried, 0.25-in. o.d. Pyrex tube, which was cooled in liquid N_2 and then sealed off under a vacuum of 10^{-8} Torr. The tube containing the RuF_5 was set up vertically and the bottom heated to 65 °C in an oil bath. Crystals suitable for X-ray studies grew by sublimation over several days. Selected crystals were inserted into nominally 0.3-mm quartz capillaries which had been drawn down further to provide for the tight fit of such small crystals. The crystal used in the data collection is described in Table SI, where other pertinent data are also given.

Structure Refinement. The habit of the selected crystal already showed its monoclinic symmetry, with well-developed faces. From the carefully measured intensities, structure factors were derived by routine methods.[26] For absorption correction, ψ-scans of 11 reflections were taken in steps of $\Delta\psi = 10°$. As one of these reflections (115) showed a completely different intensity distribution, it was remeasured with $\Delta\psi = 2°$. This

Table I. Crystallographic Data for $(RuF_5)_4$

chem formula	RuF_5	fw	196.062
a,[a] Å	5.4967 (3)	space group[b]	$P2_1/c$ (No. 14)
b, Å	9.9459 (4)	λ, Å	Mo Kα (0.710 69)
c, Å	12.5278 (6)	ρ_{calcd}, g cm^{-3}	3.861
β, deg	99.958 (2)	μ, cm^{-1}	45.4
V, Å^3	674.57	R[c]	0.0236 (0.0295)[d]
Z	8	R_w	0.0200 (0.0211)
T, °C	20		

[a] Unit cell parameters and their esd's were derived by a least-squares fit to the setting angles of the unresolved Mo Kα components of 25 reflections with 2θ between 30.3 and 37.2°. [b] International Tables for X-ray Crystallography; Kynoch: Birmingham, England, 1965; Vol. 1. [c] The quantity minimized in the least-squares procedures is $\sum w(|F_o| - |F_c|)^2$. $R = \sum w||F_o| - |F_c||/\sum|F_o|$; $R_w = \{\sum w(|F_o| - |F_c|)^2/\sum wF_o^2\}^{1/2}$. [d] R values for all unique reflections including those "unobserved" are given in parentheses.

(9) Claassen, H. H.; Selig, H.; Malm, J. G.; Chernick, C. L.; Weinstock, B. *J. Am. Chem. Soc.* **1961**, *83*, 2390. Weinstock, B.; Claassen, H. H.; Chernick, C. L. *J. Chem. Phys.* **1963**, *38*, 1470.
(10) (a) Holloway, J. H.; Peacock, R. D.; Small, R. W. H. *J. Chem. Soc.* **1964**, 644.
(11) Holloway, J. H.; Peacock, R. D. *J. Chem. Soc.* **1963**, 3892.
(12) Hepworth, M. A.; Jack, K. H.; Peacock, R. D.; Westland, G. J. *Acta Crystallogr.* **1957**, *10*, 63.
(13) Tressand, A.; Bartlett, N. Unpublished observation, 1973.
(14) Gortsema, F. P.; Didchenko, R. *Inorg. Chem.* **1965**, *4*, 182.
(15) Schäfer, H.; Schnering, H. G.; Niehuess, K. J.; Nieder-Verenholz, H. G. *J. Less Common Met.* **1965**, *9*, 95.
(16) Hoppe, R.; Dahne, W. *Naturwissenschaften* **1962**, *49*, 254.
(17) Žemva, B.; Luter, K.; Jesih, A.; Casteel, W. J., Jr.; Bartlett, N. *J. Chem. Soc., Chem. Commun.* **1989**, 346.
(18) Wright, A. F.; Fender, B. E. F.; Bartlett, N.; Leary, K. *Inorg. Chem.* **1978**, *17*, 748.
(19) Rao, P. R.; Tressaud, A.; Bartlett, N. *J. Inorg. Nucl. Chem., Suppl.* **1976**, 23. Bartlett, N.; Tressaud, A. *C. R. Hebd. Seances Acad. Sci.* **1974**, *C278*, 1501.
(20) Mitchell, S. J.; Holloway, J. H. *J. Chem. Soc.* **1971**, 2789.
(21) Holloway, J. H.; Peacock, R. D. *J. Chem. Soc.* **1963**, 527.
(22) Hepworth, M. A.; Peacock, R. D.; Robinson, P. L. *J. Chem. Soc.* **1954**, 4835.
(23) Becker, S.; Müller, B. G. *Angew. Chem., Int. Ed. Engl.* **1990**, *29*, 406.
(24) Sladky, F. O.; Bullmer, P. A.; Bartlett, N. *J. Chem. Soc. A* **1969**, 2179.
(25) Žemva, B.; Lutar, K.; Jesih, A.; Casteel, W. J., Jr.; Wilkinson, A. P.; Cox, D. E.; Von Dreele, R. B.; Borrmann, H.; Bartlett, N. *J. Am. Chem. Soc.* **1991**, *113*, 4192.
(26) Sheldrick, G. M. SHELXTL-PLUS, Release V4.1 for Seimens R3m/V Crystallographic System. Analytical X-ray Instruments, Inc., Madison, WI, 1990.

Table II. Atomic Coordinates ($\times 10^5$) and Equivalent Isotropic Displacement Coefficients ($Å^2 \times 10^4$) for $(RuF_5)_4$

	x	*y*	*z*	*U*(eq)[a]
Ru1	315 (2)	24 605 (1)	−380 (1)	241 (1)
Ru2	30 528 (2)	50 037 (1)	20 015 (1)	240 (1)
F1	−9 391 (23)	16 685 (15)	−13 316 (9)	385 (3)
F2	19 051 (22)	10 664 (14)	5 134 (11)	407 (4)
F3	26 338 (21)	32 807 (15)	−4 923 (1)	366 (3)
F4	−26 460 (22)	18 299 (14)	4 755 (10)	374 (3)
F5	9 429 (20)	34 622 (13)	13 530 (8)	314 (3)
F6	19 974 (18)	59 322 (12)	5 784 (8)	292 (3)
F7	48 454 (23)	64 546 (16)	24 921 (9)	416 (4)
F8	55 896 (21)	42 635 (15)	14 388 (10)	379 (3)
F9	38 766 (23)	40 844 (15)	32 452 (9)	391 (3)
F10	2 923 (21)	56 927 (16)	24 231 (9)	368 (3)

[a] Equivalent isotropic *U* defined as one-third of the trace of the orthogonalized U_{ij} tensor.

Table III. Interatomic Distances and Bond Angles in $(RuF_5)_4$

Interatomic Distances (Å)			
Ru1–F1	1.798 (1)	Ru2–F5	2.007 (1)
Ru1–F2	1.793 (1)	Ru2–F6	2.003 (1)
Ru1–F3	1.821 (1)	Ru2–F7	1.795 (1)
Ru1–F4	1.817 (1)	Ru2–F8	1.823 (1)
Ru1–F5	1.995 (1)	Ru2–F9	1.796 (1)
Ru1–F6	1.999 (1)	Ru2–F10	1.824 (1)
Angles (deg)			
F1–Ru1–F2	93.99 (6)	F5–Ru2–F6	86.20 (4)
F1–Ru1–F3	92.36 (6)	F5–Ru2–F7	175.67 (5)
F1–Ru1–F4	92.04 (6)	F5–Ru2–F8	87.83 (5)
F1–Ru1–F5	175.50 (6)	F5–Ru2–F9	90.21 (5)
F1–Ru1–F6′	89.08 (5)	F5–Ru2–F10	87.30 (6)
F2–Ru1–F3	92.12 (6)	F6–Ru2–F7	89.51 (5)
F2–Ru1–F4	92.47 (6)	F6–Ru2–F8	88.00 (5)
F2–Ru1–F5	90.51 (5)	F6–Ru2–F9	176.41 (5)
F2–Ru1–F6′	176.93 (5)	F6–Ru2–F10	87.54 (5)
F3–Ru1–F4	173.40 (6)	F7–Ru2–F8	92.62 (6)
F3–Ru1–F5	87.54 (5)	F7–Ru2–F9	94.08 (6)
F3–Ru1–F6′	87.61 (5)	F7–Ru2–F10	91.93 (6)
F4–Ru1–F5	87.68 (5)	F8–Ru2–F9	92.00 (6)
F4–Ru1–F6′	87.55 (5)	F8–Ru2–F10	173.60 (5)
F5–Ru1–F6′	86.42 (4)	F9–Ru2–F10	92.16 (6)
Ru1–F5–Ru2	140.83 (6)	Ru2–F6–Ru1′	136.80 (6)

proved that the crystal in its particular orientation showed serious secondary diffraction (Renniger effect). Therefore, the whole data set was carefully inspected by comparing symmetry-equivalent reflections to take care of this problem. The starting parameters for the refinement of the Ru atoms were taken as published in ref 20. A Fourier difference map revealed the positions of all 10 F atoms. The refinement including anisotropic thermal parameters and an isotropic extinction correction proceeded without any problems. Final quality factors are given in Table I, and final parameters, in Table II.

Description of the RuF_5 Structure. The structure is no different, qualitatively, from that derived originally[10,20] by Holloway and his coworkers. It consists of tetrameric units closely-packed such that the F ligand arrangement is almost that of a hexagonal-close-packed array. The greater precision now attained clearly differentiates the bridge Ru–F interatomic distances from the nonbridging and accurately defines the coordination sphere about each Ru atom. The distances and angles of chemical interest are given in Table III. Figure 1 illustrates the tetramer geometry, with Ru–F interatomic distances and Ru–F–Ru bridging angles specified.

It is seen that the six F ligands about each Ru atom are in approximately octahedral array, a cis pair of F atoms being each shared with another Ru atom, such linkages forming the tetrameric ring. The bridging Ru–F distances range from 1.995 (1) to 2.007 (1) Å, these being barely significantly different from 2.000 Å. The nature of the puckering of the ring results in opposite pairs of Ru–F–Ru angles in the tetramer being physically akin. The reentrant pair, with bridging F ligands in van der Waals contact, have an angle of 136.80 (6)°. The other bridging angle is slightly larger at 140.83 (6)°.

The nonbridging Ru–F distances are geometrically classified into two significantly different sets. Those nonbridging Ru–F trans to the bridges are shorter than those perpendicular to the plane containing each Ru

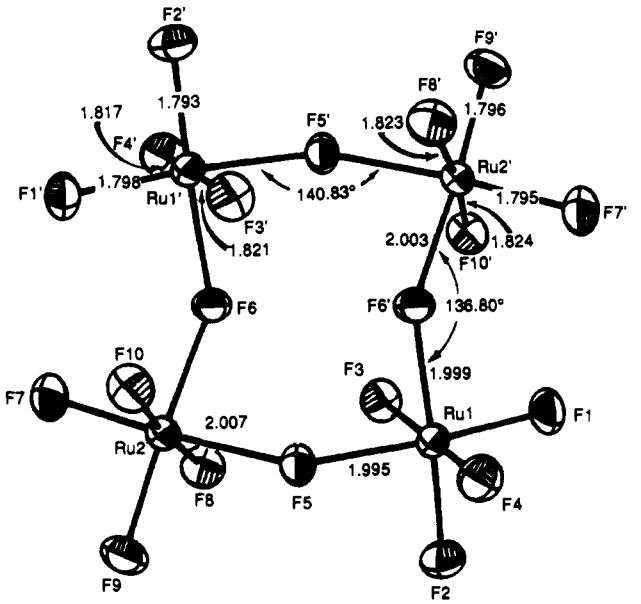

Figure 1. Tetrameric structural unit of $(RuF_5)_4$ (70% probability ellipsoids) with interatomic distances (Å) and bridge-bonding angles (deg).

atom and its bridging F ligands. The distances for the former range from 1.793 (1) to 1.798 (1) Å, whereas the latter values span 1.817 (1)–1.824 (1) Å. There are slight but significant departures from an octahedral framework, the two nonbridging Ru–F trans to the bridges subtending an angle at the Ru atom significantly greater than 90°, the pair of bridging F atoms subtending an angle correspondingly less than 90°. In addition the nonbridging F atoms normal to the plane, defined by the Ru atom and its bridging F ligands, are displaced slightly along the bisector of the angle subtended by the Ru–F bridging atoms. These angle deformations and displacements are consistent with ligand–ligand repulsive interactions, those associated with the shortest Ru–F being strongest and those with the longest Ru–F (the bridging distances) being weakest.

RuF_4 Preparation and Structure. Preparation. K_2RuF_6 was prepared in two ways. One was as previously described.[22] The second employed RuF_5 (q.v.) and KF in AHF to yield $KRuF_6$. The $KRuF_6$ was reduced by KBr in AHF ($KRuF_6 + KBr \rightarrow K_2RuF_6 + {}^1/_2Br_2$). The K_2RuF_6 X-ray powder diffraction patterns from the two syntheses were identical. RuF_4 was derived from K_2RuF_6 in an all Teflon apparatus. This consisted of two $^3/_8$-in. o.d. FEP tubes, each sealed at one end and joined at right angles to a Teflon Swagelock T compression fitting, which was also attached to a Teflon valve. This T assembly was joined to the gas handling and vacuum system via a 1-ft length of 0.25-in. i.d. FEP tubing to provide for the decantation of AHF solutions from one of the legs of the T into the other. All Teflon apparatus was dried at ~20 °C under vacuum (10^{-3} Torr) for several hours and then exposed to AHF, which had itself been dried over K_2NiF_6, this AHF then being discarded. K_2RuF_6 (600 mg; 2 mmol) was dissolved in AHF (2 mL) at ~20 °C in one leg of the apparatus, and AsF_5 gas was slowly admitted (slow addition giving a more crystalline product) to precipitate a deep-pink solid. This solid was washed 10 times with AHF by decantation, followed by back distillation of the AHF, under vacuum, into the limb of the Teflon T containing the solid. This provided for removal of the $KAsF_6$ formed in the reaction. Although PF_5 proved to be ineffective in forming RuF_4, it giving rise to a dark-brown solution (probably of RuF_5^-) and KPF_6, it was useful in combination with AsF_5, the product being somewhat more crystalline than with AsF_5 alone. For this combined PF_5/AsF_5 procedure, the solution of K_2RuF_6 in AHF was first treated with PF_5 until PF_5 uptake ceased, and then AsF_5 was introduced and the mixture was stirred (with a Teflon-coated magnet) at 20 °C for several hours, the precipitated solid being a homogeneous deep pink in color. To analyze the pink solid, it was decomposed in aqueous sodium hydroxide, F^- in the filtrate being determined as PbClF. The hydrated dioxide of the metal was filtered off and ignited in hydrogen to the metal. Anal. Found: F, 42.1; Ru, 57.7. Calcd for RuF_4: F, 42.9; Ru, 57.1. X-ray powder patterns of the RuF_4 prepared in this way proved to be the same as those of the RuF_4 phase present in the product of the reduction of $(RuF_5)_4$ with Ru metal or RuF_3.[13]

Structure of RuF_4. Data Collection. Synchrotron powder X-ray diffraction data were collected on a sample of RuF_4 contained in a 0.5-

Table IV. RuF_4 X-ray Synchrotron Data Collection

instrument employed	Brookhaven National Laboratory, National Synchrotron Light Source, beam line X7A
sample capillary	RuF_4 contained in 0.5-mm diameter quartz
wavelength	λ = 1.248 05 Å from a Si(111) channel cut monochromator
diffraction geometry	Debye–Scherrer, with a 0.55-mm receiving slit 70 cm from the sample
data range	13.0–58.4° in 0.04° steps with 64 contributing reflections

mm diameter quartz capillary using beam line X7A at Brookhaven National Laboratory (details in Table IV). Additionally, time-of-flight powder neutron diffraction data were collected on approximately 50 mg of material contained in a 2-mm diameter quartz capillary using the high-intensity powder diffractometer (HIPD) at Los Alamos National Laboratory.[27] The availability of instruments such as HIPD, with very high neutron flux and medium resolution, allows the study of small samples, such as those required for work in special environments or where there are sample handling and synthesis difficulties. The neutron data were collected for 20 h with the source operating at a proton current of 90 mA. Normally a period of 1–2 h would be used for the collection of data from a much larger sample (typically 5–10 g of material); consequently, the present data are of considerably lower statistical quality than that usually obtained.

Data Analysis. The Bragg peaks resulting from the main phase in the powder X-ray pattern had a fwhm of at least 0.24°. The peaks due to the presence of a small amount of $KAsF_6$ were considerably sharper and were comparable with the instrumental resolution (approximately 0.09°). The first 16 peak positions in the X-ray data excluding those from $KAsF_6$ were located precisely using a least squares fitting procedure and were used as input for the auto indexing program[28] TREOR. The best solution was a monoclinic cell with a = 5.614 (1) Å, b = 4.9508 (7) Å, c = 5.414 (1) Å, β = 121.41 (2)°, and M_{16} = 49 (ref 29) giving Z = 2. The observed systematic absences were consistent with the space group $P2_1/n$, but a space group could not be unambiguously assigned due to the small range of well-resolved data. The program[30] GSAS was used for further analysis. The Ru atoms were assigned to a special position in the space group $P2_1/n$ and the fluorine atoms located in a Fourier difference map. The resulting model was then refined using the Rietveld method[31] to give a chemically plausible structure but a poor fit to the diffraction pattern. A more crystalline RuF_4 sample containing less $KAsF_6$ impurity was prepared for the neutron diffraction work using PF_5 in combination with AsF_5 (q.v. preparation). Neutron diffraction data were collected using this sample.

The X-ray structural model was used as a starting point for the time-of-flight powder neutron diffraction data. This analysis employed the data collected on the +153, −153, and −90° banks of the instrument HIPD, the resolution of the lower angle banks being too low to warrant inclusion in the refinement. The count rate in the +90° bank appeared to be anomalously low; hence, these data were excluded from the refinement. A refinement using a cosine Fourier series background was performed but did not produce a satisfactory background fit. Subsequently the background was modeled assuming that it contained a contribution due to scattering from an amorphous component; the resulting fit was improved, but the refined background parameters had no physical significance. An unrestrained refinement including all positional parameters and isotropic temperature factors was initially performed. A second refinement which included restraints on the Ru–F distances (bridging Ru–F distance 2.00 Å and terminal Ru–F distance 1.82 Å) was then carried out. The results of both refinements are given in Table V, and the interatomic distances and angles are given in Table VI for comparison. The fitted neutron time-of-flight powder diffraction data are shown in Figure 2. There is no sigificant difference in the quality of the fit for either of these models as judged by the profile R factors, but the R_F's (the normal crystallographic R factors) appear to be significantly lower for the restrained model. The slightly better compatibility of the diffraction data, with the restrained model, is also evident from the lower esd's on the coordinates and bond lengths from that refinement.

The observed Debye–Scherrer data together with relative intensities calculated for the restrained model are given in Table VII, and the structure is illustrated in Figure 3.

RuF_3 Preparation and Structure. Preparation. The ability of SF_4 to act as a reducing agent[32] and as a scavenger of oxygen by exchanging fluorine for oxygen[33] recommended its employment in the reduction of RuF_5 to produce RuF_3. The likelihood that SF_4 would form a salt SF_3-

Table V. Comparison of the Restrained (r) and Unrestrained (u) Refinements of the Structural Models for RuF_4 in Space Group $P2_1/n$[a,b]

	R factors			
	R_{wp}, %	R_p, %	R_F, %	
−90° bank (including 233 reflcns)	4.53	2.81	5.06	u
	4.54	2.81	4.90	r
+153° bank (including 630 reflcns)	3.12	2.14	17.20	u
	3.13	2.14	15.25	r
−153° bank (including 629 reflcns)	3.42	2.33	14.26	u
	3.43	2.34	13.31	r

	x	y	z	$100U_{iso}$, Å^2	
Ru1	0.0	0.0	0.0	1.98 (9)	u
				2.02 (9)	r
F1	0.8662 (24)	0.1523 (11)	0.2231 (10)	2.0 (1)	u
	0.8762 (10)	0.1498 (9)	0.2212 (8)	1.6 (1)	r
F2	0.3636 (24)	0.1674 (9)	0.2485 (10)	1.7 (1)	u
	0.3736 (6)	0.1696 (6)	0.2509 (8)	1.8 (1)	r

[a] a = 5.6068 (6) Å, b = 4.9456 (5) Å, c = 5.413 (2) Å, and β = 121.27 (2)°. [b] Overall X^2 = 1.388 for the free refinement and 1.397 for the restrained refinement.

Table VI. Interatomic Distances (Å) and Angles (deg) in RuF_4

	model	
	unrestrained	restrained
2 × Ru1–F1	1.88 (2)	1.82 (1)
2 × Ru1–F2	1.95 (3)	2.00 (3)
2 × Ru1–F2	2.02 (1)	2.00 (1)
F1–Ru1–F2	89.4 (6)	89.7 (6)
F1–Ru1–F2	88.2 (4)	89.3 (2)
F2–Ru1–F2	89.2 (12)	90.3 (12)
F1–Ru1–F2	90.6 (6)	90.3 (6)
F1–Ru1–F2	91.8 (4)	90.7 (2)
F2–Ru1–F2	90.8 (12)	89.7 (12)
Ru1–F2–Ru1	134.9 (8)	133.0 (6)

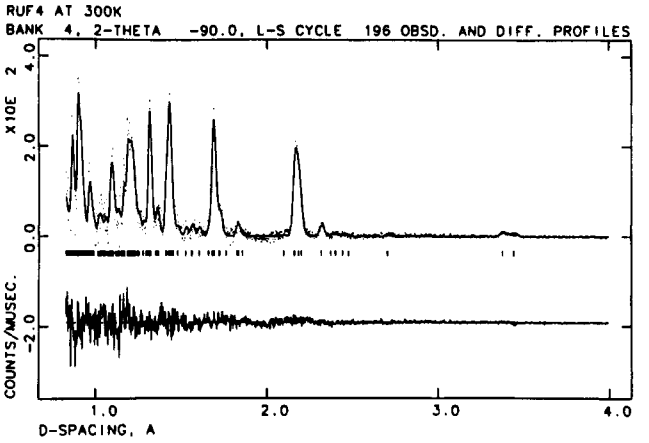

Figure 2. Observed neutron time-of-flight powder diffraction data minus the calculated background shown as dots. The calculated values from the constrained model with bridging M–F = 2.00 Å and nonbridging M–F = 1.82 Å are shown as a curve. A difference ($I_{obs} - I_{calc}$) curve and the reflection positions are also shown.

(27) Myer, D. K., Ed. Condensed Matter Research of LANSCE. Los Alamos Laboratory Report LALP 90-7, Jan 1990, pp 10–11.
(28) Werner, P. E.; Eriksson, L.; Westdahl, M. J. *J. Appl. Crystallogr.* **1985**, *18*, 367.
(29) De Wolff, P. M. *J. Appl. Crystallogr.* **1968**, *1*, 108.
(30) Larson, A. C.; Von Dreele, R. B. Los Alamos Laboratory Report, No LAUR86-748, 1990.
(31) Rietveld, H. M. *J. Appl. Crystallogr.* **1968**, *2*, 65.
(32) Bartlett, N.; Hepworth, M. A. *Chem. Ind.* **1956**, 1425.
(33) Hasek, W. R.; Smith, W. C.; Engelhardt, V. A. *J. Am. Chem. Soc.* **1960**, *82*, 539.

Table VII. X-ray Powder Data (Cu Kα Radiation, Ni Filter) for the RuF_4 Monoclinic Unit Cell Indexed on the Basis of the Unit Cell Parameters from the Neutron Diffraction Data[a]

		$1/d^2 \times 10^4$		
I/I_0	I_{calc}	obs	calc	*hkl*
vs	100	430	434	$10\bar{1}$
vs	~0	840	843	$11\bar{1}$
	83		844	110
vs	81	877	876	011
m	22	1374	1371	101
w	7	1640	1635	020
w	11	1675	1681	$21\bar{1}$
s	11	1739	1738	$20\bar{2}$
	14		1741	200
ms	24	1774	1776	$11\bar{2}$
	~0		1779	111
vvw	1	1869	1868	002
m	19	2053	2070	$12\bar{1}$
	~0		2071	120
m	9	2095	2102	021
m	8	2146	2146	$21\bar{2}$
	8		2150	210
	~0		2277	012
	~0		2907	$22\bar{1}$
	~0		2978	$30\bar{2}$
ms	6	2999	2981	$30\bar{1}$
	~0		3003	$12\bar{2}$
	13		3006	121
vvw	4	3240	3235	$10\bar{3}$
	11		3372	$22\bar{2}$
s (br)	10	3391	3377	220
	9		3387	$31\bar{2}$
	~0		3390	$31\bar{1}$
m	15	3503	3504	022
s (br)	17	3656	3546	$21\bar{3}$
	17		3554	211
w	~0	3656	3644	$11\bar{3}$
	9		3649	112

[a] $a = 5.6068$ (6), $b = 4.9456$ (5), $c = 5.413$ (2) Å, $\beta = 121.27$ (2)°, $V = 128.3$ Å^3, $Z = 2$, space group $P2_1/n$.

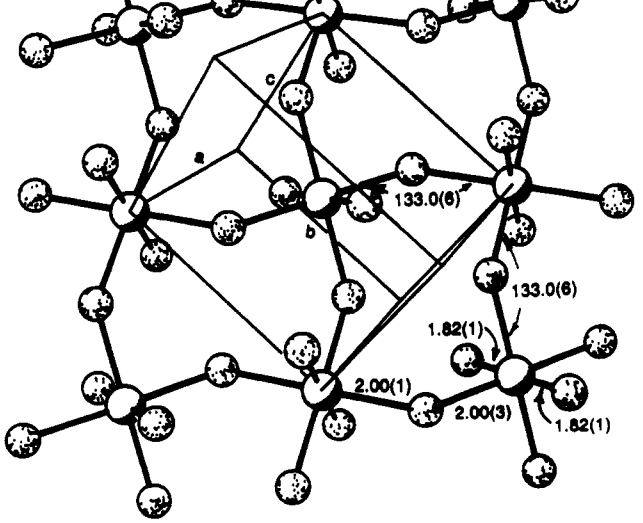

Figure 3. View of the puckered-sheet structure of RuF_4 with interatomic distances (Å) and bridge-bonding angles (deg).

RuF_6, analogous to those already known for Sb,[34] Os, and Ir[35] was also an important consideration, since there was then the possibility of deriving the RuF_3 in one step from the reductive breakdown of the lattice of the salt: $SF_3RuF_6 \rightarrow SF_6 + RuF_3$. A preliminary experiment was conducted in a KelF reactor (previously loaded with RuF_5 in the Dri-lab). SF_4 was added to a maximum pressure of 2.5 atm, with the RuF_5 in the tube heated to 125 °C. The SF_4 supply was maintained until a homogeneous pink-tinged white solid was obtained. This gave a simple X-ray powder diffraction photograph related to those with cubic patterns[34,35] obtained from SF_3MF_6 (M = Sb, Ir, Os). The pattern was indexed on a tetragonal cell (Table VIII), the volume of which is consistent with the formulation SF_4RuF_5. Larger quantities of the adduct were prepared by heating the RuF_5 (~3 g) at ~140 °C, with a large excess of SF_4 (~15 atm) for 3 h in a 200-mL capacity, all-welded Monel can ($^1/_{32}$-in. wall) provided with a removable lid sealed to the body with a Teflon gasket. The lid and gasket were cooled (by water or compressed air) when the vessel was heated. A dome, soldered to the lid, and a hollow collar, attached to the Teflon-gasketed flange, provided for this. An X-ray photograph of the nearly white product confirmed that it was all of the tetragonal SF_4RuF_5 phase. The can with ~5 g of adduct was filled with SF_4 to ~5 atm and heated at ~470 °C for 15 h with water cooling of the flange and dome. A dark brown solid lay on the bottom of the reactor. Analysis by pyrohydrolysis proved it to be RuF_3. Anal. Found for Ru: (1) 63.7; (2) 63.9. Calcd for RuF_3: Ru, 63.9.

Table VIII. X-ray Powder Diffraction Data (Cu Kα Radiation, Ni Filter) for SF_3RuF_6 with a Body-Centered Tetragonal Cell[a]

	$1/d^2 \times 10^4$		
hkl	calc	obs	I/I_0
002	298	299	s
200	347	347	s
211	508	512[b]	w
202	645	642	vs
220	694	693	s
222	992	999	m
213	1105	1107[b]	w
004	1192	1196	m
400	1388	1396	vvw
204	1539	1541	m
330	1562		
420	1735	1739	w
323	1799	1789[b]	vw
224	1886	1890	w
422	2033	2024	w
510	2256	2258[b]	vw
215	2297	2298[b]	vw
404	2580	2574	w
440	2776	2780	vw
424	2927	2939	w (br)
206	3029	3064	w (br)
226	3376	3383	w (br)

[a] $a = 10.73$ (1), $c = 11.58$ (1) Å, $Z = 8$, $V = 1334$ Å^3. [b] These reflections require the large cell, otherwise $a = 5.365$ Å, $c = 5.79$ Å, and $Z = 1$.

RuF_3 Structure. X-ray powder diffraction photographs using LiF-monochromatized Cu Kα radiation were sharp and of low background. The patterns were indexed completely on the basis of a rhombohedral cell (see Table IX), and refinement yielded unit cell parameters with $a = 5.4098$ (4) Å and $\alpha = 54.67$ (1)° slightly larger (but not significantly so) than those preferred by Jack and his co-workers[12] as "ideal" for the composition RuF_3, of $a = 5.408 \pm 0.001$ Å and $\alpha = 54.67 \pm 0.01$°. The relative line intensities obtained here were not significantly different from those given by Jack and his co-workers. After application of the positional parameter found by Jack and his co-workers ($x = -0.100$, for which 3σ is ≤ 0.005) to their cell, the Ru–F interatomic distance is 1.981 (6) Å. With the cell parameters found in this work, Ru–F = 1.982 (6) Å. The Ru–F–Ru bridging angle found here is 136 (1)°.

Discussion

The interatomic distances and bond angles in the RuF_5 tetramer (see Table III and Figure 1) are now defined with high precision. The bridging Ru–F interatomic distances are all nearly the same and barely significantly different from 2.000 Å. Although it cannot be said that the bridging distance is significantly longer than that in RuF_3 (which Ru–F distance we now know must be 1.982 (6) Å), that is what was expected on the basis of the comparison of $(RhF_5)_4$ with RhF_3. Longer

(34) Bartlett, N.; Robinson, P. L. *J. Chem. Soc.* **1961**, 3417.
(35) Jha, N. K. Ph.D. Thesis, University of British Columbia, 1965. Gibler, D. D.; Adams, C. J.; Fischer, M.; Zalkin, A.; Bartlett, N. *Inorg. Chem.* **1972**, 2325.

Table IX. X-ray Powder Data (Cu Kα Radiation, LiF Monochromator) for RuF_3 with a Rhombohedral Unit Cell[a]

	$1/d^2 \times 10^4$		
I/I_0	obs	calc	hkl[b]
10	757	751	110
6.5	1400	1385	211
4	1635	1620	$10\bar{1}$
1	1920	1902	222
4	2114	2095	201*†
5	2389	2371	200
5	3030	3005	220
10	3545	3522	321
		3833	$20\bar{1}$*
4	3945	3921	332
6	4015	3991	$21\bar{1}$
6	4650	4625	310
6	4877	4860	$2\bar{1}\bar{1}$
		5100	320*
4	5554	5541	422
4	5842	5822	433
1	5937	5898	432*†
		6368	421*
3	6492	6480	$20\bar{2}$
3	6778	6761	330, 411
1	6974	6955	$31\bar{1}$*†
		7073	$2\bar{2}1$*
6	7183	7160	431
6	7240	7231	$30\bar{1}$
4	7447	7442	442
3	7610	7606	444
5	7864	7865	$32\bar{1}$
		8340	410*
6	8384	8381	420
3	8829	8851	$22\bar{2}$
4	9057	9062	532
4	9226	9226	543
3	9491	9485	400
		9608	430*
		10171	542*
		10313	$30\bar{2}$*
5	10400	10400	521
4	10479	10471	$31\bar{2}$
		10758	531*†
3	10900	10893	554
4	11106	11105	$41\bar{1}$
4	11346	11340	$3\bar{2}\bar{1}$
		11580	$42\bar{1}$
1	11817	11815	$32\bar{2}$, $40\bar{1}$*†
3	12030	12020	440
5	12292	12302	541
7	12475	12466	633, 552
		12513	644
		12707	643*
		12848	520*
10	13243	13241	$43\bar{1}$, 510
		13411	632*
		13505	654*†
7	13647	13640	530
		13711	$\bar{4}11$
5	13933	13922	622
7	14088	14086	642
6	14125	14133	653
4	14348	14345	$33\bar{2}$
5	14579	14580	$30\bar{3}$
		15055	$4\bar{2}1$*†
6	15328	15331	$40\bar{2}$
6	15543	15542	631
		15618	540*†
5	15697	15679	664
		15947	652*
6	15964	15965	$4\bar{2}2$
		16440	$5\bar{1}1$*
5	16477	16481	$52\bar{1}$

[a] a = 5.4098 (4) Å, α = 54.68 (1)°, V = 98.08 Å^3, Z = 2, space group $R\bar{3}c$. [b] Asterisks indicate fluorine-only reflections ($h + k + l$ = odd), and daggers indicate fluorine-only reflections for which $h + k + l = 3(2n + 1)$.

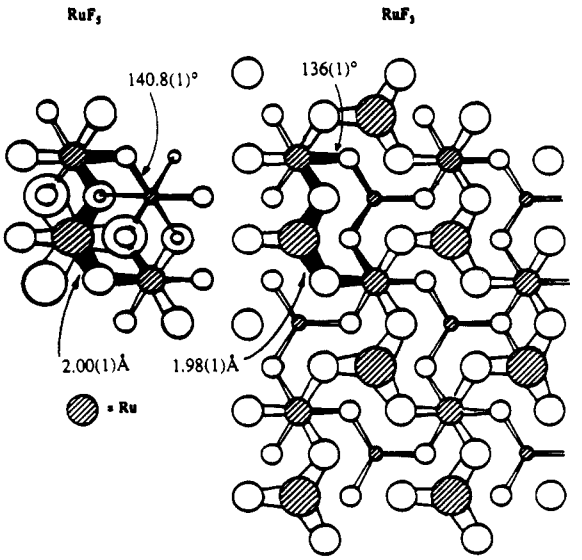

Figure 4. Relationship of the $(RuF_5)_4$ geometry to an element of the RuF_3 infinite hexagonal nearly-close-packed F atom array.

bridging interatomic distances, M–F_b, in the pentafluoride than in the trifluoride may simply arise from cis-F-ligand repulsions. This, surprisingly, sets aside any impact of changes in the d electron configuration and allows that all M–F_b distances (for given M) could be intrinsically the same and independent of oxidation state. Those repulsions experienced by the bridging F ligands in the pentafluoride are greater than in the trifluoride. This is a consequence of four nonbridging M–F distances at ~1.8 Å in the pentafluoride, whereas all six M–F lengths in the trifluoride are at ~2.0 Å. Small differences aside, the bridging M–F bonds in the pentafluoride and trifluoride of both Ru and Rh are unexpectedly similar.

The similarity of the pentafluoride and trifluoride bridge bonding leads to a close correspondence in the way the ruthenium atoms occupy octahedral sites in the approximately hexagonally close-packed F ligand array that occurs in both fluorides.[10,12,20] Figure 4 compares the RuF_5 tetramer with an element of the RuF_3 infinite array, which is seen to be almost identical in conformation. As Jack and his co-workers had pointed out,[12] however, in their original structure determination of RuF_3, their diffraction data clearly established that the F ligand array is not exactly hexagonal-close-packed, the bridging angle being 136°, and not 132°, which is the angle required for exact close packing. In RhF_3 on the other hand,[5,12] the Rh–F–Rh bridge angle is close to the theoretical one for close packing. The bridging angles in $(RhF_5)_4$, which are 134.35 (10) and 135.71 (11)°, are also closer to the ideal hexagonal close packing than those found in $(RuF_5)_4$, which are 136.80 (6) and 140.83 (6)°. Evidently a change in the nature of the M–F–M bonding constrains the bridging angle to be larger in the ruthenium case. A bridging angle closer to 136° than to 132° seems to be required for Ru–F–Ru. This is probably a consequence of less covalency in the Ru case, relative to Rh, because of the lower nuclear charge in Ru.

The nonbridging Ru–F distances in $(RuF_5)_4$ are in two distinct sets (see Figure 1). The nonbridging F ligands, trans to the bridging F ligands (termed "equatorial" here), are significantly closer to the Ru atom than are the nonbridging ligands (termed "axial") perpendicular to the plane, containing the Ru atom and its bridging F ligands. The distances for the former range from 1.793 (1) to 1.798 (1) Å, whereas for the latter the range is 1.817 (1) to 1.824 (1) Å. This is the inverse of the situation pertaining in the RhF_5 tetramer,[6] where the Rh–F nonbridging distances trans to the bridging F ligands range from 1.810 (4) to 1.820 (4) Å and those perpendicular to the plane, defined by the Rh atom and its bridging-F ligands, range from 1.796 (4) to 1.803 (4) Å. These small but significant differences, between the $(RuF_5)_4$ and

$(RhF_5)_4$ structures, must be tied to the different "d orbital" populations of the two materials. The lowest lying orbital, which is of π^* character (derived from the approximately-dt_{2g} orbitals of the metal and the F $p\pi$ orbitals) must be located in the plane of the M atom and its two bridging-F ligands. In Rh(V), which has a d^4 configuration, this orbital will be fully occupied. This will mean that the F ligands trans to the bridging F ligands in $(RhF_5)_4$ experience more π^* character than do the nonbridging F perpendicular to the bridging-ligand plane, since the appropriate π^* orbitals there will only be singly occupied. This accounts for the $(RhF_5)_4$ nonbridging Rh–F distances being slightly longer in the equatorial plane. But the $(RuF_5)_4$ findings are not so easily accounted for. The d^3 configuration of Ru(V), with its preference for singly occupied orbitals of the t_{2g} set in O_h symmetry, indicates that all of the nonbridging F ligands would experience the same π^* effect of that configuration. The bridging-F ligands, however, must be more electron rich than their nonbridging counterparts and can be viewed as on the ionization pathway toward F^-. The other electron clouds, proximate to the Ru atom and in the same plane as the Ru atom and its bridging-F ligands, will under those circumstances contract toward the Ru atom. Perhaps it is simply this trans electrostatic effect which causes the observed shortening of the trans set of nonbridging Ru–F distances, there now being only one π^* electron in the equatorial plane. But these are all subtle effects, since the difference between the two sets of nonbridging F ligands is only about 0.03 Å.

Unfortunately, the Ru–F distance in RuF_6 is not known, but an estimate can be made of it. Levy et al.[36] have determined the Mo–F distance in cubic MoF_6 to be 1.802 (14) Å, which is not significantly different from the more precise distance of 1.820 (3) Å derived by Seip and Seip[37] from an electron diffraction study of MoF_6 gas. Siegel and Northrop[38] have given the unit cell dimensions for all of the second transition series hexafluorides, as well as those of the third series, in both the cubic and orthorhombic forms. If all of the contraction in volume in passing from cubic MoF_6 to cubic RuF_6, were taken up in bond contraction (treating the molecules as spheres), the Ru–F interatomic distance would be 1.77 Å on the basis of the 1.820 (3) Å distance for MoF_6. This of course assumes that the van der Waals radius of the F ligand in RuF_6 is the same as in MoF_6. That this may not be accurately so is indicated by the electron diffraction results of Kimura et al.[39] on the third transition series set, where the interatomic distances (Å) were found to be W–F = 1.833 (4), Os–F = 1.831 (4), and Ir–F = 1.830 (4). The unit cell data of Siegel and Northrop[4] applied similarly, in comparison of IrF_6 and WF_6, predict Ir–F = 1.818 Å on the basis of 1.833 Å for WF_6. The Ru–F distance in RuF_6 could, therefore, be slightly larger than 1.77 Å, but it cannot be greater than that for Mo–F in MoF_6. The axial nonbridging Ru–F distances in $(RuF_5)_4$ are therefore seen to be slightly longer than that anticipated for the hexafluoride although those trans to the bridging F ligands must be nearly the same as Ru–F in RuF_6.

Although the diffraction data available from RuF_4 are of low quality, probably as a result of the small crystallite size, consequent on the method of preparation, some firm structural conclusions can be drawn. The structure is of the same type as VF_4 derived by Becker and Müller from single-crystal studies.[23] The two Ru atoms in the monoclinic unit cell are at 0, 0, 0 and $^1/_2$, $^1/_2$, $^1/_2$, the Ru–Ru distances then being simply determined by the unit cell dimensions, which are accurately defined. From this, each Ru atom is seen to have four close Ru atom neighbors in a roughly square arrangement in the same plane. This Ru–Ru nearest-neighbor distance of 3.664 (2) Å is close to that observed in RuF_3, where Ru–Ru = 3.672 (4) Å, and to the adjacent Ru atom distances in $(RuF_5)_4$, where Ru–Ru = 3.7207 (2) and 3.7705 (2) Å. This at once suggests a similarity in the bridge-bonding in all three fluorides.

The Fourier difference map for RuF_4 clearly indicated a roughly octahedral arrangement of six F ligands about each Ru atom with four, in the same plane, making bridge bonds to the four nearest-neighbor Ru atoms. The low quality of the data did not provide for precise location of the light atoms, however, and as Table V shows, a constrained model, based on Ru–F distances, anticipated from the findings on RuF_3 and $(RuF_5)_4$, provided slightly better agreement than the unaided refinement. Figure 3 illustrates the puckered sheet structure of RuF_4, as defined by the restrained model in which each bridging Ru–F distance was fixed at 2.00 Å and the nonbridging Ru–F distances (which are normal to the bridging Ru–F) were constrained to be 1.82 Å. The refinement has disposed the F ligands to produce the particular puckered sheet geometry shown, with sheets packed so that the nonbridging F ligands of one sheet pack into the holes available in the nonbridging F array of an adjacent sheet. Indeed the structure is a puckered version of that adopted[14,15] by NbF_4, which has the same structure as SnF_4.[16] The puckering of the sheet is simply a consequence of the nonlinearity of the Ru–F–Ru bridge and the octahedral framework on which the six F ligands lie about each Ru atom. The puckered eight-membered ring unit, seen in the RuF_4 sheet structure, is strikingly similar to the RuF_5 tetramer illustrated in Figure 1. Certainly, an "ideal" RuF_4 sheet structure can be built up, which exactly meets the unit cell dimensions and symmetry, by close-packing sheets made by extending the $(RuF_5)_4$ ring system indefinitely. For that extension into sheets, the nonbridging Ru–F trans to the bridging Ru–F, of the $(RuF_5)_4$ ring, now become bridging ligands. Because of the octahedral framework about each Ru, a Ru–F–Ru bridge which is exo, in one of the eight membered rings, has a cis F ligand on the same Ru atom subtend an endo Ru–F–Ru bridge in the same ring. A trans F ligand, on the same Ru atom, has its Ru–F–Ru angle kinked oppositely to its relative in the adjacent eight-membered ring.

The restraints of 2.00 Å for the bridging and 1.82 Å for the nonbridging Ru–F distances in RuF_4 resulted in the highly plausible geometry illustrated in Figure 3. The resultant bridging angle of 133.0 (6)° is, however, a little smaller than anticipated, on the basis of the RuF_3 and $(RuF_5)_4$ findings. If the bridging Ru–F distance were to be intermediate between the values observed in RuF_3 and $(RuF_5)_4$, i.e. 1.99 Å rather than the 2.00 Å assumed, then the bridging Ru–F–Ru angle would be 134°. This angle becomes 135° if the Ru–F distance is the same as in RuF_3.

As may be seen from the available data for the second transition series binary fluorides illustrated in Figure 5, the approximate lack of dependence of the M–F bond character (whether bridging or nonbridging) on the oxidation state of M appears to hold for the fluorides of Nb and Mo as well as those of Ru and Rh. As better precision is attained, for the structures of the pentafluorides of Nb and Mo, it is highly probable that this approximate constancy of M–F bond character will be affirmed. There are, however, some subtle dependencies on oxidation state which deserve comment.

In each case the bridging distance in the trifluorides of Nb, Mo, Ru, and Rh are quoted to be shorter than that for the corresponding distance in the pentafluoride. This difference is significant in the case of Rh, is nearly so for Ru, and appears likely to be real for the others also. Because the trifluoride of an element has two more π^* electrons than a pentafluoride, M–F_b in the former ought to be weaker, and the interatomic distances longer, than in the latter. The reverse situation is observed. It appears, therefore, that the impact of F···F nearest-neighbor

(36) Levy, J. H.; Sanger, P. L.; Taylor, J. C.; Wilson, P. W. *Acta Crystallogr.* **1974**, *B31*, 1065.
(37) Seip, H. M.; Seip, R. *Acta Chem. Scand.* **1966**, *20*, 2699.
(38) Siegel, S.; Northrop, D. A. *Inorg. Chem.* **1966**, *5*, 2187.
(39) Kimura, M.; Schomaker, V.; Smith, D. W.; Weinstock, B. *J. Chem. Phys.* **1968**, *48*, 4001.
(40) LaValle, D. E.; Steele, R. M.; Wilkinson, M. K.; Yakel, H. R., Jr. *J. Am. Chem. Soc.* **1960**, *82*, 2433.

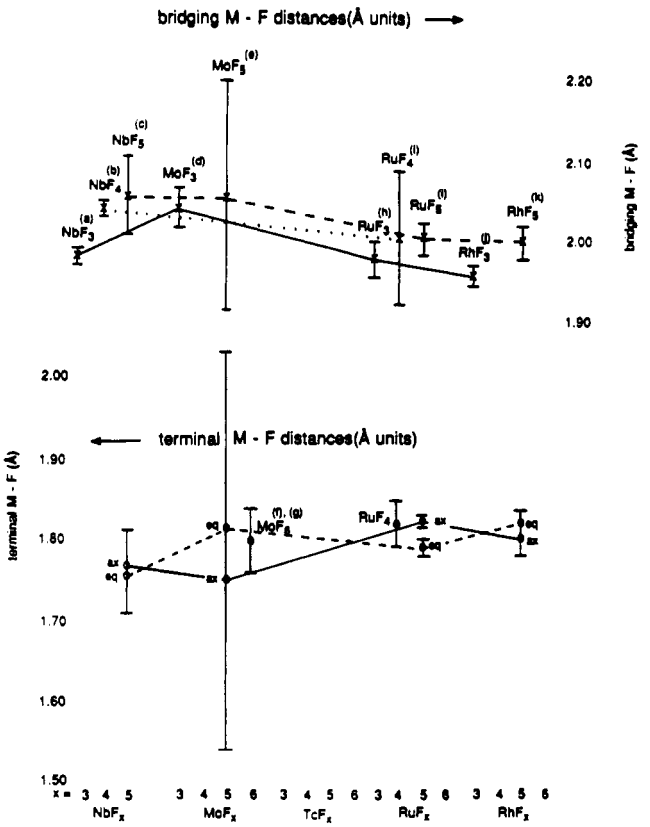

Figure 5. M–F interatomic distances, terminal and bridging (Å) for the binary fluorides of Nb through Rh (error bars represent $\pm 3\sigma$). Reference key for footnotes: a, 7; b, 14 and 15; c, 8; d, 40; e, 41; f, 36; g, 37; h, 12; i, present work; j, 5; k, 6.

repulsions is more important than changes in the d electron configuration. The bridging M–F distances in the pentafluoride appear to be stretched as a consequence of the greater repulsive effect on each F_b of the three cis nonbridging M–F ligands. There may be a parallel dependence of nonbridging M–F distances upon the number of bridging ligands.

The M–F nonbridging distances in the pentafluorides are all close to 1.8 Å (Nb through Rh). None is significantly longer than Mo–F in MoF_6, the electron-diffraction result[37] for that gaseous molecule being 1.820 (3) Å. Indeed the average nonbridging M–F distances (albeit imprecise) in MoF_5[41] and NbF_5[8] are respectively 1.78 and 1.77 Å. This is consistent with two of the F ligands in the pentafluorides having a bridging role (and hence M–F ≈ 2.0 Å) and this diminishing the repulsive interactions experienced by the four nonbridging F ligands. If this is generally true, the M–F distances in the hexafluorides should all prove to be slightly longer than the average nonbridging M–F distances in their pentafluoride relatives. This of course supposes that the F···F interactions remain more important than changes in the π^* electron configuration. There are indications in the data presented in Figure 5 and the π^* configuration does have subtle impact however.

The nonbridging M–F distances in the pentafluorides which are trans to the bridging F ligands are labeled equatorial, and those perpendicular to the plane, defined by the M atom and its bridging F, are labeled axial. As has already been discussed, the greater length of the equatorial nonbridging M–F distance in RhF_5 can be attributed to the filled π^* orbital in the equatorial plane. In MoF_5, also, we anticipate the occupied π^* orbital (one electron) to be located in that plane. Thus, the quotation that the Mo–F equatorial distance is greater than the Mo–F axial distance (although not significantly so) may prove to be real, in which case a weak π^* effect will have been substantiated. In NbF_5, with no π^* electrons, and RuF_5 with equal occupancy of the π^* orbitals (t_{2g}^3 configuration) the axial bonds are slightly longer (although in the former case not significantly so) that the equatorial, probably from the trans effect of the bridging F, as already discussed.

It is highly probably that a similar approximate independence of the M–F distances from oxidation state will apply also in the third transition series binary fluorides, in all of those cases (which is the majority[4]) where σ^* electrons are not involved. High-precision data are, however, harder to obtain with those heavier elements.

Acknowledgment. The work was supported by the Chemical Sciences Division of the U.S. Department of Energy under Contract No. DE-AC03-67SF0098. Additional support was provided by the U.S.-Yugoslav Joint Fund for Scientific and Technological Cooperation in association with the National Science Foundation under Grant No. JF947. The work pertaining to RuF_3 was supported by the National Science Foundation at Princeton University (1988–9). We are also grateful to Dr. David Cox of the Department of Physics, Brookhaven National Laboratory, Upton, Long Island, NY, and Dr. Robert B. Von Dreele, of the Manuel Lujan, Jr., Neutron Scattering Center, Los Alamos National Laboratory, Los Alamos, NM, for their valuable assistance in the collection of diffraction data from RuF_4 samples. H.B. also gratefully acknowledges the Alexander von Humboldt Foundation for a Feodor Lynen Fellowship. A.P.W. thanks the SERC for a Studentship, Christ Church College Oxford for a scholarship, Shell, Amsterdam, for funding, and Dr. A. K. Cheetham for valuable discussions.

Supplementary Material Available: Tables SI and SII, listing crystal data and details of data collection and anisotropic displacement coefficients for RuF_3 (3 pages). Ordering information is given on any current masthead page.

(41) Edwards, A. J.; Peacock, R. D.; Small, R. W. H. *J. Chem. Soc.* **1962**, 4486.